Interfacial toughening of solution processed Ag nanoparticle thin films by organic residuals

2012 Nanotechnology 23 485704

(http://iopscience.iop.org/0957-4484/23/48/485704)

Nanotechnology **23** (2012) 485704 (8pp) doi:10.1088/0957-4484/23/48/485704

Interfacial toughening of solution processed Ag nanoparticle thin films by organic residuals

Inhwa Lee[1,3], Sanghyeok Kim[1,3], Jeonghoon Yun[1], Inkyu Park[1,2] and Taek-Soo Kim[1,2]

[1] Department of Mechanical Engineering, KAIST, Daejeon 305-701, Korea
[2] KI for the NanoCentury, KAIST, Daejeon 305-701, Korea

E-mail: inkyu@kaist.ac.kr and tskim1@kaist.ac.kr

Received 14 May 2012, in final form 23 September 2012
Published 6 November 2012
Online at stacks.iop.org/Nano/23/485704

Abstract
Reliable integration of solution processed nanoparticle thin films for next generation low-cost flexible electronics is limited by mechanical damage in the form of delamination and cracking of the films, which has not been investigated quantitatively or systematically. Here, we directly measured the interfacial fracture energy of silver nanoparticle thin films by using double cantilever beam fracture mechanics testing. It was demonstrated that the thermal annealing temperature and period affect the interfacial fracture energy. Also it was found that the interfacial fracture resistance can be maximized with optimized annealing conditions by the formation of organic residual bridges during the annealing process.

S Online supplementary data available from stacks.iop.org/Nano/23/485704/mmedia

(Some figures may appear in colour only in the online journal)

1. Introduction

Solution-based direct metal printing methods [1–7] without conventional microfabrication processes (for example photolithography and vacuum deposition processes such as evaporation or sputtering) are attracting significant attention as the next generation manufacturing processes for low-cost electronics applications. Gold or silver nanoparticles from a few to tens of nanometers in size are typically used as the materials for metal nanoparticle-based ink solutions in the fabrication of printed flexible electronics. These metal nanoparticles have a lower melting temperature than that of bulk material due to the large surface-to-volume ratio [7, 8]. Also, the electrical conductivity of nanoparticle-based thin films can be raised to values similar to the bulk after a sintering process at low temperature (150–250 °C) for tens of minutes [2, 7, 9, 10]. Therefore, in recent years, various printing methods such as inkjet printing [1, 2], gravure/flexography printing [3–5], and nanoimprinting [6, 7] of metal nanoparticle solutions have been developed for micro/nano-scale direct metal patterning. In addition, other solution-based patterning methods such as micromolding in capillaries (MIMIC) [11, 12], nanoembedding [13], and lithographically controlled wetting (LCW) [14] have been developed for micro/nano-scale patterning of metal nanoparticles. These solution-based printing processes have advantages such as simple equipment, high fabrication speed, lower material consumption, and low manufacturing cost compared to conventional metallization methods based on vacuum systems.

In flexible electronics, large deformation caused by severe mechanical loading such as repeated bending, twisting or stretching has emerged as a fatal problem [15] because it causes cracking and delamination of thin films from flexible substrates. Furthermore, mismatch of coefficients of thermal expansion (CTE) for metal thin film and polymer substrates may expedite these mechanical failures by temperature swings during the fabrication process and in-service operation. Accordingly, work has been done on measuring the mechanical properties of metal nanoparticle films, such as

[3] These authors contributed equally to this work.

hardness and elastic modulus, by the nanoindentation test [16, 17] and strain sensitivity by the tension test [18]. However, to the best of our knowledge, quantitative and systematic research on diagnosing and improving the adhesion of nanoparticle-based thin films to the substrate has not been conducted so far, although qualitative methods such as the tape test [19] and shear test [20] have been used to examine the adhesion properties. An in-depth understanding of the adhesion properties of metal nanoparticle films is essential both for the manufacturing process and real-life device applications. The adhesion energy can be measured by various techniques including the peel test [21], the die shear test [20], the four point bending (FPB) test [22], and the double cantilever beam (DCB) method [23–25]. Since the DCB test is a mode I opening, it is especially appropriate for measuring the adhesion energy of various thin films such as nanoporous organosilicate thin films [25] and graphene layers [26] which cannot be accurately measured by other methods.

In the present study, we used the DCB method to quantify the interfacial fracture energy of solution processed Ag nanoparticle thin films on the silicon substrate. Using the DCB test we demonstrated how the thermal annealing temperature and period affect the interfacial fracture energy of Ag nanoparticle thin films, and found that the interfacial fracture resistance can be maximized with optimized annealing conditions with organic residuals at the interface. Surprisingly, it was also found that the organic residuals segregated onto the substrate during the annealing process and formed an organic bridge [27, 28] which is believed to strengthen the interface between the silver nanoparticle film and the substrate.

2. Experiment

The interfacial fracture energy was measured by DCB fracture mechanics testing [23–25]. Nanoparticle-based silver ink (DGP 40LT-15C, Advanced Nano Products, Korea) was spin-coated onto the silicon substrate at 5000 rpm for 30 s. The nanoparticle size was 30–50 nm and the metal content of the silver nanoparticle ink was 35 wt% in methyl alcohol solvent. The transmission electron microscopy (TEM) image provided by the manufacturer is shown in figure S1 of the supplemental materials (available at stacks.iop.org/Nano/23/485704/mmedia). These nanoparticles were uniformly dispersed in the solvent with a low viscosity (10–17 cP) for printed electronics applications and the surface tension of nanoparticle ink was 35–38 mN m^{-1}. The nanoparticle is encapsulated by a polymer shell that was revealed in other work as polyvinylpyrrolidone (PVP) [29, 30], as was also confirmed by our Fourier transform infrared spectroscopy (FT-IR) analysis shown in figure S2 of the supplemental materials (available at stacks.iop.org/Nano/23/485704/mmedia). The PVP shell is expected to melt and form organic residuals on the surface of the silicon substrate by thermal annealing at temperatures above 150 °C, because the melting temperature of PVP is 150–180 °C. Then, the silver nanoparticle film was sintered in a convection oven at 150 °C for 30 min to remove the solvent and to form a solid silver thin film. After this initial sintering process, silver nanoparticle films were further annealed at various temperatures (150, 200, and 230 °C) and periods (3, 6, and 9 h). The annealing processes were performed in a convection oven in an air environment. In order to quantify the possible influence of oxidation, we conducted x-ray photoelectron spectroscopy (XPS) analysis of surfaces of silver nanoparticle thin films after annealing at the various temperatures and periods. We found that there were no significant differences in the amount of oxygen at 150 °C, regardless of the annealing period, resulting in oxygen compositions of 3.97, 3.28, and 3.71 at.% for 3, 6, and 9 h, respectively. On the other hand, at higher temperatures, more oxygen was detected with increasing annealing periods (3.81, 3.96, and 5.15 at.% for 3, 6, and 9 h, respectively, at 200 °C; 5.09, 5.70, and 6.16 at.% for 3, 6, and 9 h, respectively, at 230 °C). From these results, we could assume that the surface of silver nanoparticles was thermally oxidized only at temperatures higher than 150 °C during the annealing process. The film thickness of silver nanoparticle film was measured from its cross-sectional image by scanning electron microscopy (SEM). The measured thickness was 1 μm as shown in figure 2. After thermal annealing, the specimens were fabricated for DCB fracture mechanical testing.

A 25 nm thick Cr layer and a 75 nm thick Al layer were deposited on the silver nanoparticle film by a thermal evaporation process. This additional metal thin film structure was employed as a stiff elastic standoff layer in order to prevent plastic deformation of epoxy and associated plastic energy contributions to the interfacial fracture energy of the nanoparticle thin film [31]. Also these layers are essential for preventing the permeation of epoxy into the silver nanoparticle film. Afterwards, 353nd epoxy (Epo-Tek 353ND consisting of bisphenol F and imidazole; Epoxy Technology) with 1 μm thickness was coated on the Al layer and a dummy silicon substrate was attached for making a sandwich structure as shown in figure 1(a). The fracture mechanics testing of the DCB specimen was conducted using a high-precision micromechanical test system (Delaminator Adhesion Test System, DTS Company, USA). Figure 1(a) also shows the equipment and the loaded specimen for the DCB test. The thin films sandwiched between silicon substrates were loaded under a constant displacement rate of 2 μm s^{-1} while the applied load is continuously monitored as a function of displacement, as shown in figure 1(b). The thin film sandwiched between silicon substrates was initially loaded elastically, but once the rate of strain energy release exceeded the interfacial fracture energy of the silver nanoparticle film/silicon interface, crack growth occurred within the interface. At this critical point, the slope of the load–displacement curve starts to decrease, reflecting changes in specimen compliance with the extension of the crack. During the subsequent extension of the crack by several millimeters, the beam was partially unloaded and then subjected to further multiple instances of loading/crack-growth/unloading cycles, as shown in figure 1(b), in order to obtain multiple values for the interfacial fracture energy by

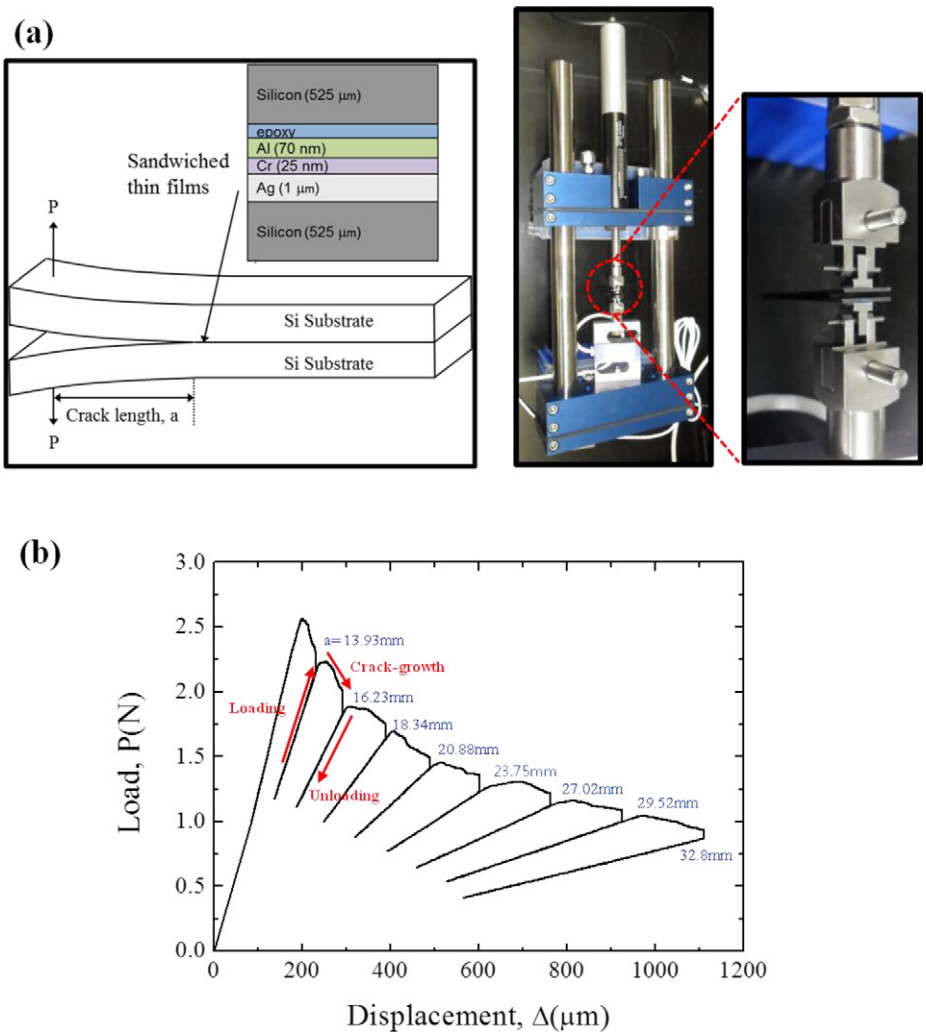

Figure 1. (a) A schematic of the DCB specimen containing a silver nanoparticle thin film sandwiched between silicon substrates and a photograph of the micromechanical test system with a specimen for the DCB test. (b) Load–displacement curve for a DCB test specimen annealed at 230 °C for 9 h. Multiple loading/crack-growth/unloading cycles were performed to measure the crack lengths and the interfacial fracture energy of the silver nanoparticle film on the silicon substrate. The measured crack length, a, for each cycle is shown.

using a compliance-based model. The interfacial crack length, a, and the adhesion energy, G_c, can be given by [23–25]:

$$a = \left(\frac{du}{dP}\right)^{1/3}\left(\frac{BE'h^3}{8}\right)^{(1/3)} - 0.64h \quad (1)$$

$$G_c = \frac{12P_c^2a^2}{E'B^2h^3}\left(1 + 0.64\frac{h}{a}\right)^2 \quad (2)$$

where du/dP is the elastic compliance, u is the total displacement of the beam ends, P is the applied load, B is the sample width, h is the half height of the substrate, E' is the plane-strain modulus of the beam, and P_c is the critical load where the slope of the load–displacement curve starts to decrease in figure 1(b).

3. Results and discussions

Figure 2 shows the SEM images of surface morphology and cross-sections of silver nanoparticle thin films that were annealed at different temperatures for various periods. After annealing at 150 °C for 3 h the thin film showed a porous surface morphology composed of silver nanoparticles with an average grain size of ∼30 nm. At 150 °C, there were almost no changes in the grain size, porosity, or connectivity between nanoparticles with longer periods of annealing. However, at higher temperatures (200 and 230 °C), continued growth and aggregation of silver nanoparticles can be clearly observed with longer annealing periods. Also, for the same annealing period, aggregation and growth of nanoparticles became more significant at higher annealing temperatures. However, from these SEM images, it was difficult to precisely determine the evolution of morphology. Only subtle differences were seemingly observed, but the details in the microstructure of the silver nanoparticle film were not clear. However, the measured interfacial fracture energy of silver nanoparticle films annealed at different temperatures for various periods clearly showed the effect of thermal annealing as shown in figure 3(a). The interfacial fracture energy between the silver nanoparticle film and the substrate was maximum and

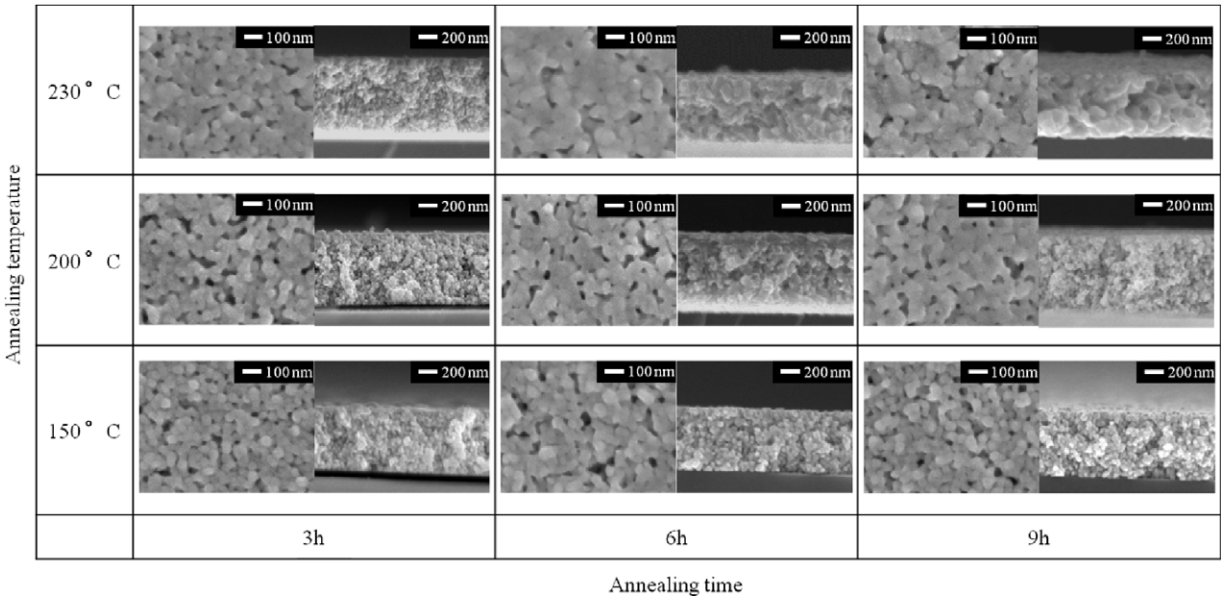

Figure 2. SEM images of surface morphologies (left) and cross-sections (right) of silver nanoparticle film on a silicon substrate annealed at various temperatures (150, 200, and 230 °C) for different periods (3, 6, and 9 h).

minimum after annealing for 6 h and 9 h, respectively, at all annealing temperatures. Also, the interfacial fracture energies of specimens annealed at temperatures above 150 °C were larger than those of specimens annealed at 150 °C, regardless of the annealing period. The maximum interfacial fracture energy was 6.49 ± 0.5 J m^{-2} after annealing at 230 °C for 6 h. On the other hand, the minimum interfacial fracture energy was 4.05 ± 0.43 J m^{-2} after annealing at 150 °C for 3 h. Here, the fracture energy was increased by 60%, from 4.05 to 6.49 J m^{-2}, by annealing. We are the first to report the interfacial fracture energies of silver nanoparticle thin films, and therefore other established or reported fracture energies for direct comparison are not available as yet. However, there are relevant reported studies suggest that an interfacial fracture energy higher than 5 J m^{-2} is required to prevent delamination and cracking of copper/low-*k* interconnects in microelectronics during harsh fabrication and packaging processes [32, 33]. Therefore, we believe that the enhancement of the interfacial fracture energy from 4.05 to 6.49 J m^{-2} in our case is critical to ensuring the mechanical reliability of various electronic devices using silver nanoparticle thin films. From these results, we could find that the interfacial fracture energy is very sensitive to the annealing temperature and period and that there is an optimal annealing condition to maximize the interfacial fracture energy between a silver nanoparticle film and substrate.

We investigated why the interfacial fracture energy is maximal after annealing for 6 h by conducting SEM imaging and XPS analysis. In the SEM images (figures 4(a)–(c)) of the surface of the silicon substrate after the completion of the DCB test, a number of residuals could be observed. Using XPS analysis, these residuals were found to mainly consist of carbon with negligible amounts of silver (table 1). We believe that these carbon residuals are precipitates of the organic shells that were originally coated on the

Table 1. XPS analysis of the surface composition of the silicon substrate after detaching the silver nanoparticle films annealed at 150 °C and 200 °C for various periods (3, 6, and 9 h), respectively.

Component (at.%)	150 °C			200 °C		
	3 h	6 h	9 h	3 h	6 h	9 h
Si 2p	94.97	88.87	96.28	75.16	25.8	89.59
Ag 3d	0	0	0	0.08	0.13	0
O 1s	2.01	2.73	1.65	7.56	8.58	3.76
C 1s	3.01	8.39	2.06	17.20	65.48	6.66

surface of nanoparticles. These organic shells are commonly used not only to prevent nanoparticles from aggregation (for high dispersion stability) but also to control the size of nanoparticles [34–36]. The reported thickness of the PVP shell surrounding nanoparticles is typically 1–2 nm as characterized by TEM [37, 38]. However, they can be melted down through a porous network of nanoparticles and precipitated to the substrate during a long-term thermal annealing process at elevated temperatures. Figures 4(a)–(c) reveal that the organic residuals on the substrate after annealing at 200 °C for 6 h remained much more than those annealed at 150 °C for 6 h and at 200 °C for 9 h. Even though gradual evaporation of the PVP organic residuals occurs at 200 °C, the PVP does not immediately decompose at that temperature. Thermogravimetric analysis (TGA) data show that a drastic mass change of the PVP shell occurs at around 450 °C [39, 40], which was also confirmed by our analysis as shown in the figure S3 in the supplemental materials (available at stacks.iop.org/Nano/23/485704/mmedia). This means that the organic residuals of the PVP shell would be retained at 200 °C, which is significantly lower than the reported decomposition temperature around 450 °C. The XPS analysis for the silicon substrate with organic residuals in figure 3(b) also presents similar trends for annealing

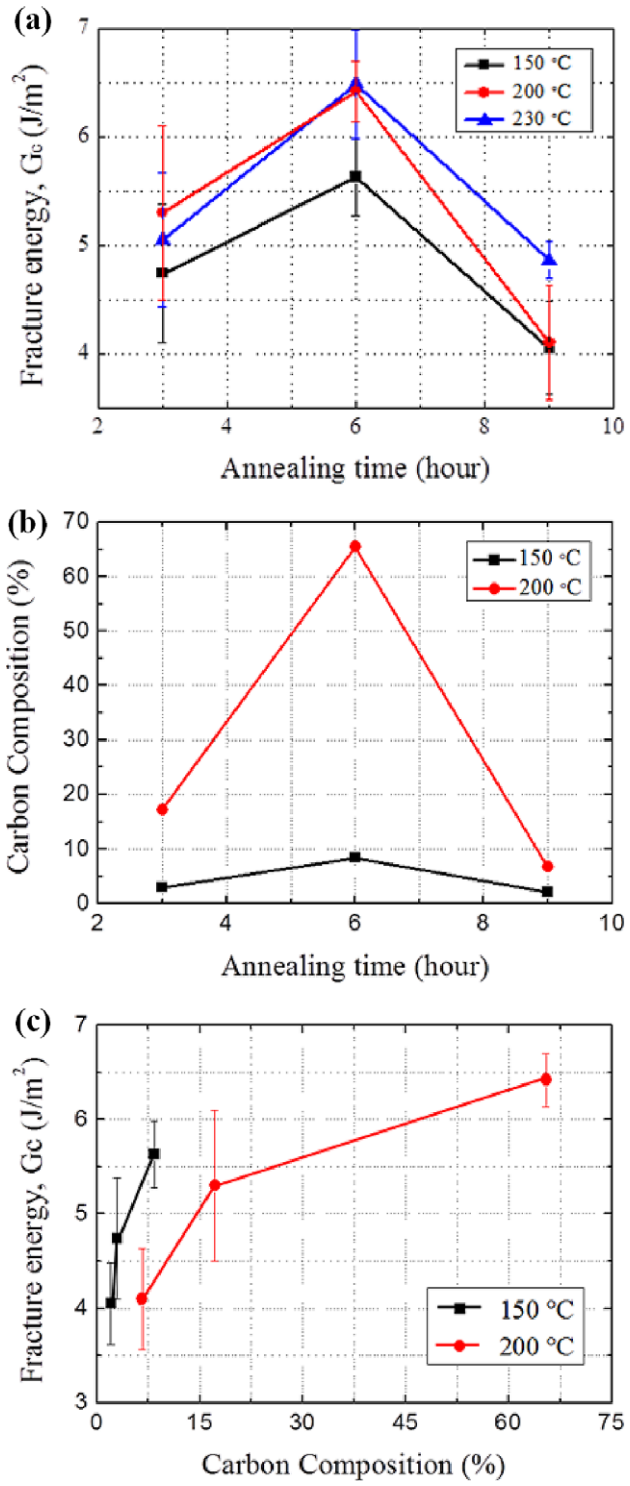

Figure 3. (a) Fracture energy measured with respect to various annealing periods and temperatures. (b) Carbon composition on the silicon substrate after detaching the silver nanoparticle film annealed at various conditions. (c) Fracture energy with respect to the remaining carbon composition on the substrate after detaching the silver nanoparticle film.

temperature and periods. The carbon composition is maximal (65.48%) for annealing at 200 °C for 6 h. At 230 °C, a cohesive failure near the interface of silver nanoparticle and substrate occurred instead of pure interfacial failure. This means that the organic residuals on the silicon substrate are buried under a skin layer of silver nanoparticles cohesively fractured from the silver nanoparticle thin film. We tried to remove the skin layer and characterize the carbon composition of the organic residuals by XPS depth profiling with an argon ion beam. However, we could not obtain the exact carbon composition at the surface because argon sputtering caused severe damage to organic materials. This problem caused by argon sputtering is expected to be solved by replacing argon with a buckminsterfullerene (C_{60}) ion beam for XPS analysis [41, 42]. Unfortunately, the XPS equipment (ESCA2000, Thermo VG Scientific, UK) used in this study did not provide a C_{60} sputtering capability. Therefore, the carbon composition data for the samples annealed at 230 °C could not be obtained for figures 3(b) and (c). In comparison, the carbon composition is 8.39% for annealing at 150 °C for 6 h, which is much lower than the maximum. It is believed that the PVP shell surrounding the nanoparticle melts and slowly precipitates onto the substrate surface at annealing temperatures above 150 °C, resulting in an increase of the carbon composition with the annealing period up to 6 h. However, excessive annealing times over 6 h would start to reduce the carbon composition by the gradual evaporation of PVP organic residuals from the interface of the Ag film and the silicon substrate. By comparing the interfacial fracture energy to both SEM images and XPS composition analysis, we can observe similar trends for annealing temperature and period.

By observing the similarity of trends for interfacial fracture energy (figure 3(a)) and for the carbon composition (figure 3(b)) with annealing temperature and period, it can be inferred that carbon residuals play a critical role in determining the interfacial fracture energy. The larger the carbon composition is, the higher the interfacial fracture energy, as shown in figure 3(c). These carbon residuals between nanoparticle thin film and substrate function as organic bridges that increase the interfacial fracture energy. The surface morphology of organic residuals is irregular with heights from 30 to 80 nm. Surface profiles obtained using an atomic force microscope (AFM) are shown in figures 4(d)–(e). These irregular morphologies of organic residuals can be attributed to the bridging phenomenon during the process of crack propagation in a nanoparticle thin film. We can envision the strengthening mechanism of interfacial fracture energy by organic residual bridging in three steps, as shown in figure 5. Firstly, organic shells are separated from silver nanoparticles and segregated onto the silicon substrate through the porous structure of the silver nanoparticle film by an additional annealing process. Secondly, the precipitated organic residuals on the substrate form organic bridges at the interface between the silver nanoparticle film and the substrate. This organic bridging strengthens the interfacial fracture energy of the silver nanoparticle film and the substrate. Lastly, the crack is further propagated after the organic bridging structures are broken by dissipating more strain energy. According to the bridging theory [43], the carbon bridging present at the interface of layered films dissipates the debonding energy by stretching

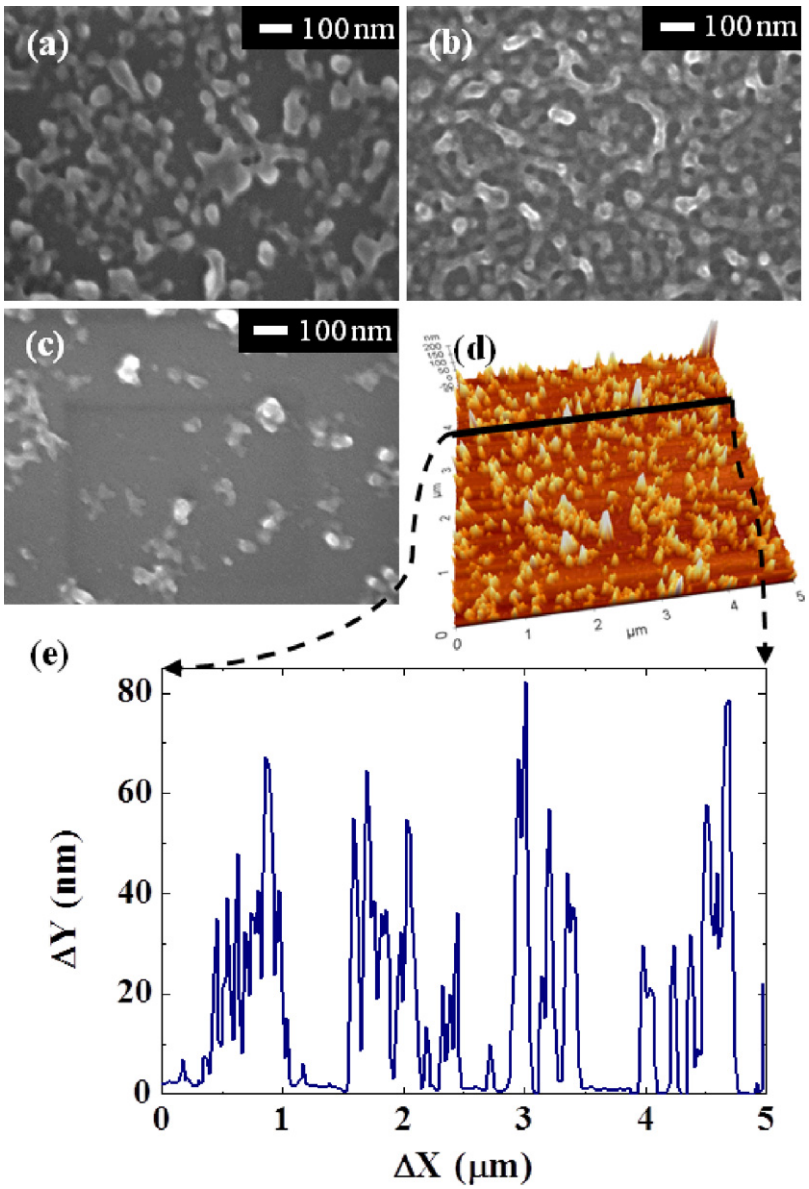

Figure 4. SEM images of the surface of the silicon substrate after detaching the silver nanoparticle film annealed at (a) 150 °C for 6 h, (b) 200 °C for 6 h, and (c) 200 °C for 9 h, respectively. (d) AFM image and (e) its line profiling of the silicon surface for the film annealed at 150 °C for 6 h.

the carbon bridging, and thus the energy to debond the crack tip is increased remarkably. The equation for the increased interfacial fracture energy, G_c, can be written as follows:

$$G_c = G_o + G_{bridging} \quad (3)$$

where G_o is the intrinsic interface fracture energy required to debond the interface and the $G_{bridging}$ is the interfacial fracture energy contributed by organic bridging. If the annealing time and temperature are less than optimal, a small amount of residual carbon at the interface results in a small interfacial fracture energy (figure 5(a)). However, if excessive annealing is applied, the amount of residual carbon is reduced by thermal decomposition, and thus the interfacial fracture energy is reduced (figure 5(c)). Therefore, in order to achieve the maximum interfacial fracture energy, optimal annealing conditions should be applied (figure 5(b)).

The marked effect of organic residuals on the interfacial fracture energy has not been previously reported for metal nanoparticle thin films. Previous studies on the annealing effect of metal nanoparticle thin film have been mainly focused on the changes in microstructure and electrical conductivity. It has been commonly known that the electrical conductivity is monotonically enhanced by annealing at higher temperatures for longer periods through better merging between individual nanoparticles and enlarging the grain sizes in the thin film [9, 10, 34–36]. However, the present work has revealed that appropriate annealing conditions enable the formation of an organic residual layer between the nanoparticle thin film and substrate and thus provide a bridging effect against the detachment of the film, resulting in an increased interfacial fracture energy. Therefore, an important conclusion from the present work is that the optimal

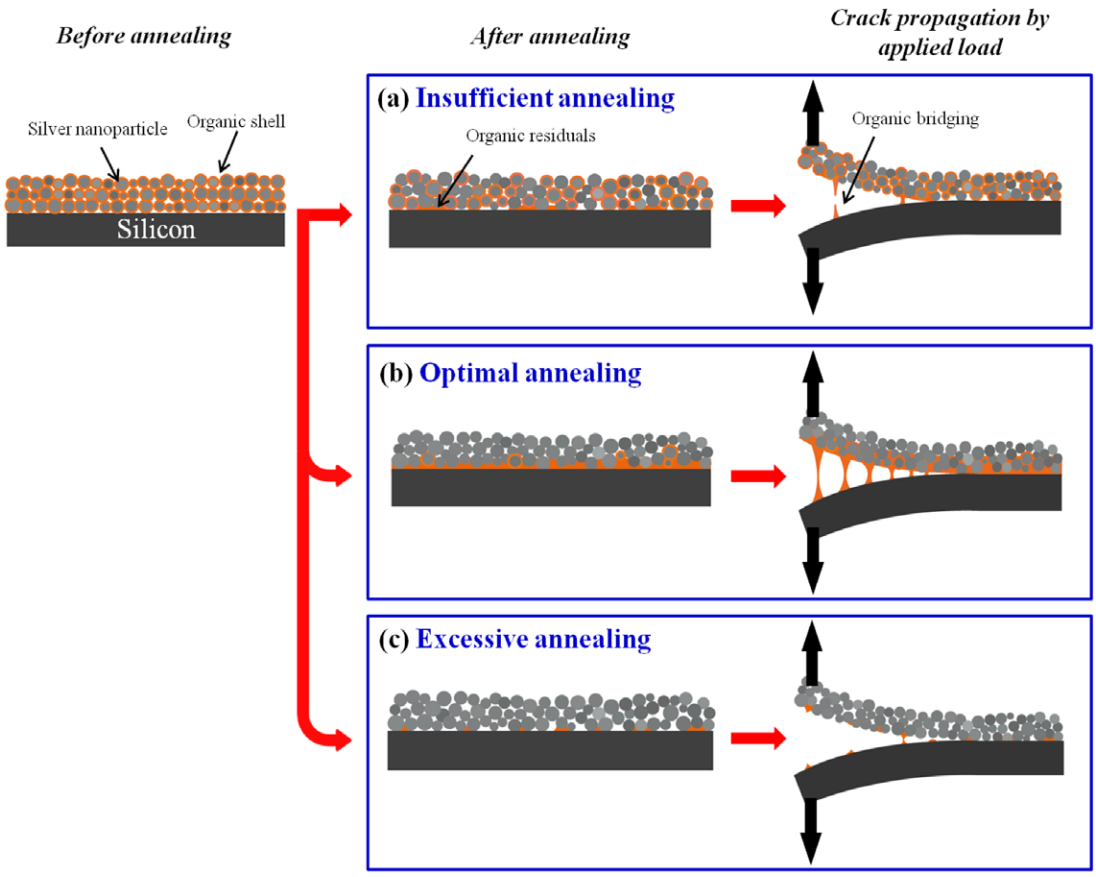

Figure 5. Schematic illustration for the mechanism of organic bridging at the interface between the silver nanoparticle film and substrate after (a) insufficient, (b) optimal, and (c) excessive annealing processes. When the annealing temperature and period are optimal, the precipitated organic residuals on the substrate form sufficient organic bridging between the nanoparticle film and substrate, which increases the interfacial fracture energy. On the other hand, the amount of residual carbon is reduced by thermal decomposition under an excessive annealing process, and this reduces the interfacial fracture energy.

annealing temperature and period should be carefully chosen in order to obtain enhanced interfacial fracture resistance as well as electrical conductivity.

In summary, we investigated the substantial effect of annealing conditions on the interfacial fracture energy of metal nanoparticle thin films on a silicon substrate and found that there is an optimal annealing condition to maximize the interfacial fracture energy. The experimental results strongly indicate that the organic residuals melted from organic shells of metal nanoparticles and segregated onto the interface strengthen the interfacial fracture energy through a bridging mechanism. We believe that this work provides a better understanding of the adhesion mechanism and interfacial fracture between metal nanoparticle thin films and substrates, and a foundation for novel methods to improve the adhesion of nanoparticle thin film by using organic components contained within the nanoparticle solution.

Acknowledgments

This research was supported by the Basic Science Research Program (2012006072), Future-based Technology Development Program (Nano Fields) (2011-0019168), and Mid-career Research Program (Key Research) (2011-0027669) through the National Research Foundation of Korea (NRF) funded by the Korean government (MEST), and the MCP Core Technologies for the Next Generation Project of the Ministry of Knowledge Economy of Korea.

References

[1] Luechinger N A, Athanassiou E K and Stark W J 2008 *Nanotechnology* **19** 445201
[2] Jeong S, Song H C, Lee W W, Choi Y and Ryu B H 2010 *J. Appl. Phys.* **108** 102805
[3] Puetz J and Aegerter M A 2008 *Thin Solid Films* **516** 4495–501
[4] Jo J, Yu J S, Lee T M and Kim D S 2009 *Japan. J. Appl. Phys.* **48** 04C181
[5] Deganello D, Cherry J, Gethin D and Claypole T 2010 *Thin Solid Films* **518** 6113–6
[6] Park I, Ko S H, Pan H, Grigoropoulos C P, Pisano A P, Fréchet J M J, Lee E S and Jeong J H 2008 *Adv. Mater.* **20** 489–96
[7] Ko S H, Park I, Pan H, Grigoropoulos C P, Pisano A P, Luscombe C K and Fréchet J M J 2007 *Nano Lett.* **7** 1869–77
[8] Buffat P and Borel J 1976 *Phys. Rev.* A **13** 2287
[9] Kim I, Song Y A, Jung H C, Joung J W, Ryu S S and Kim J 2008 *J. Electron. Mater.* **37** 1863–8

[10] Russo A, Ahn B Y, Adams J J, Duoss E B, Bernhard J T and Lewis J A 2011 *Adv. Mater.* **23** 3426–30
[11] Cavallini M, Albonetti C and Biscarini F 2009 *Adv. Mater.* **21** 1043–53
[12] Cavallini M, Bystrenova E, Timko M, Koneracka M, Zavisova V and Kopcansky P 2008 *J. Phys.: Condens. Matter* **20** 204144
[13] Cavallini M, Simeone F C, Borgatti F, Albonetti C, Morandi V, Sangregorio C, Innocenti C, Pineider F, Annese E and Panaccione G 2010 *Nanoscale* **2** 2069–72
[14] Cavallini M and Biscarini F 2003 *Nano Lett.* **3** 1269–71
[15] Lee J H, Kim N R, Kim B J and Joo Y C 2011 *Carbon* **50** 98–106
[16] Greer J R and Street R A 2007 *J. Appl. Phys.* **101** 103529-5
[17] Mueggenburg K E, Lin X M, Goldsmith R H and Jaeger H M 2007 *Nature Mater.* **6** 656–60
[18] Herrmann J, Müller K H, Reda T, Baxter G, Raguse B, De Groot G, Chai R, Roberts M and Wieczorek L 2007 *Appl. Phys. Lett.* **91** 183105
[19] Joo S and Baldwin D F 2010 *Nanotechnology* **21** 055204
[20] Joo S C and Baldwin D F 2010 *IEEE Trans. Adv. Packag.* **33** 48–57
[21] Song J and Yu J 2002 *Acta Mater.* **50** 3985–94
[22] Dauskardt R, Lane M, Ma Q and Krishna N 1998 *Eng. Fract. Mech.* **61** 141–62
[23] Hohlfelder R J, Maidenberg D A, Dauskardt R H, Wei Y and Hutchinson W 2001 *J. Mater. Res.* **16** 243–55
[24] Kanninen M 1973 *Int. J. Fract.* **9** 83–92
[25] Kim T S, Tsuji N, Matsushita K, Kobayashi N, Chumakov D, Geisler H, Zschech E and Dauskardt R H 2008 *J. Appl. Phys.* **104** 074113
[26] Yoon T, Shin W C, Kim T Y, Mun J H, Kim T S and Cho B J 2012 *Nano Lett.* **12** 1448–52
[27] Gandhi D D, Lane M, Zhou Y, Singh A P, Nayak S, Tisch U, Eizenberg M and Ramanath G 2007 *Nature* **447** 299–302
[28] Maidenberg D A, Volksen W, Miller R D and Dauskardt R H 2004 *Nature Mater.* **3** 464–9
[29] Allen M, Leppaniemi J, Vilkman M, Alastalo A and Mattila T 2010 *Nanotechnology* **21** 475204
[30] Andersson H, Lidenmark C, Öhlund T, Örtegren J, Manuilskiy A, Forsberg S and Nilsson H E 2012 *IEEE Trans. Compon. Packag. Manuf. Technol.* **2** 342–8
[31] Lane M, Dauskardt R H, Vainchtein A and Gao H 2000 *J. Mater. Res.* **15** 2758–69
[32] Andideh E, Scherban T, Sun B, Blaine J, Block C and Jin B 2001 *Proc. IEEE Int. Interconnect Techonology Conf.* pp 257–9
[33] Chiu C, Chang H, Lee C, Hsia C and Chiang K 2007 *Microelectron. Reliab.* **47** 1506–11
[34] Bakhishev T and Subramanian V 2009 *J. Electron. Mater.* **38** 2720–5
[35] Jeong S, Song H C, Lee W W, Choi Y, Lee S S and Ryu B H 2010 *J. Phys. Chem.* C **114** 22277–83
[36] Jung J K, Choi S H, Kim I, Jung H, Joung J and Joo Y C 2008 *Phil. Mag.* **88** 339–59
[37] Hu A, Guo J, Alarifi H, Patane G, Zhou Y, Compagnini G and Xu C 2010 *Appl. Phys. Lett.* **97** 153117
[38] Yan J, Zou G, Wu A, Ren J, Hu A and Zhou Y 2012 *Scr. Mater.* **66** 582–5
[39] Carotenuto G, Pepe G and Nicolais L 2000 *Eur. Phys. J.* B **16** 11–7
[40] Hsu S L C and Wu R T 2010 *Int. Conf. on Nanotechnology and Biosensors IPCBEE* 2 pp 55–8
[41] Chen Y Y, Yu B Y, Wang W B, Hsu M F, Lin W C, Lin Y C, Jou J H and Shyue J J 2008 *Anal. Chem.* **80** 501–5
[42] Sanada N, Yamamoto A, Oiwa R and Ohashi Y 2004 *Surf. Interface Anal.* **36** 280–2
[43] Bao G and Suo Z 1992 *Appl. Mech. Rev.* **45** 355–66